Experimentally exploring the conformational space sampled by domain reorientation in calmodulin

Ivano Bertini*†, Cristina Del Bianco*, Ioannis Gelis‡, Nikolaus Katsaros‡, Claudio Luchinat§, Giacomo Parigi§, Massimiliano Peana¶, Alessandro Provenzani*, and Maria Antonietta Zoroddu¶

*Centre for Magnetic Resonance and Department of Chemistry, University of Florence, Via Luigi Sacconi 6, I-50019 Sesto Fiorentino, Italy; ‡National Centre for Scientific Research Demokritos, Institute of Physical Chemistry, 15310 Agia Paraskevi Attikis, Greece; §Centre for Magnetic Resonance and Department of Agricultural Biotechnology, University of Florence, Piazzale delle Cascine 28, I-50144 Florence, Italy; and ¶Department of Chemistry, University of Sassari, Via Vienna 2, 07100 Sassari, Italy

Edited by Harry B. Gray, California Institute of Technology, Pasadena, CA, and approved March 5, 2004 (received for review December 24, 2003)

The conformational space sampled by the two-domain protein calmodulin has been explored by an approach based on four sets of NMR observables obtained on Tb^{3+}- and Tm^{3+}-substituted proteins. The observables are the pseudocontact shifts and residual dipolar couplings of the C-terminal domain when lanthanide substitution is at the N-terminal domain. Each set of observables provides independent information on the conformations experienced by the molecule. It is found that not all sterically allowed conformations are equally populated. Taking the N-terminal domain as the reference, the C-terminal domain preferentially resides in a region of space inscribed in a wide elliptical cone. The axis of the cone is tilted by ≈30° with respect to the direction of the N-terminal part of the interdomain helix, which is known to have a flexible central part in solution. The C-terminal domain also undergoes rotation about the axis defined by the C-terminal part of the interdomain helix. Neither the extended helix conformation initially observed in the solid state for free calcium calmodulin nor the closed conformation(s) adopted by calcium calmodulin either alone or in its adduct(s) with target peptide(s) is among the most preferred ones. These findings are unique, both in terms of structural information obtained on a biomolecule that samples multiple conformations and in terms of the approach developed to achieve the results. The same approach is in principle applicable to other multidomain proteins, as well as to multiple interaction modes between two macromolecular partners.

Calmodulin (CaM) is a paradigm case in structural biology. The following brief survey of the history of the structural and dynamic studies on this protein serves the double purpose of putting the present findings in proper perspective and of acknowledging those pieces of previous information that were essential to allow the present approach to be developed and to yield novel structural information.

CaMs are two-domain proteins belonging to the large family of EF-hand proteins (1–3). They contain ≈150 amino acid residues, organized into two domains of ≈70 aa each and connected by a short linker. Each domain is made up of two special helix–loop–helix motifs (EF-hand motifs) that can bind a calcium ion in the loop. The two loops are held close to one another by two short antiparallel β-strands forming a three-hydrogen bond stretch of β-sheet. The function of CaM in cell cytoplasm is that of responding to sudden rises of calcium concentration by binding up to four calcium ions in the four EF-hand loops, by changing conformation because of metal binding, and by thus becoming able to recognize, bind to, and activate, a number of proteins and enzymes (1, 4–8). Early x-ray data (9) showed the four-calcium $(Ca_2)_N(Ca_2)_C$CaM form (subscripts N and C refer to the calcium atoms bound by the N- and C-terminal domains, respectively) to have a dumbbell shape, with helix 4, the last helix of the N-terminal domain, and helix 5, the first helix of the C-terminal domain, together with the interdomain linker, forming a long continuous helical structure (Fig. 1*A*). On the other hand, the protein takes up a closed conformation, with total loss of the helical character of the interdomain linker, when it binds to its target peptide(s) (Fig. 1*B*) (10–15). This binding involves the two domains getting closer to one another and clamping the recognition peptide in the target molecule between their exposed hydrophobic cores.

It was soon recognized that the NMR properties of $(Ca_2)_N(Ca_2)_C$CaM in solution were inconsistent with the rigid dumbbell shape observed in the early x-ray work, and that the central part of the helix loses its helical character and allows reciprocal reorientation of the two domains (16–20). Molecular dynamics simulations were performed (21, 22), confirming the flexibility of the two domains. An extended model-free analysis characterized the relative motions as occurring on a time scale of ≈3 ns, with a squared order parameter of 0.7 relative to the x-ray conformation, at room temperature (17). When temperature was raised to ≈40°C, a larger interdomain motion was observed, as a result of a doubling of the random coil residues in the central linker (23). Disorder in the central part of the interdomain helix was recently observed in an x-ray structure at 1.0-Å resolution (24). Finally, recent work has shown that native calcium-loaded CaM can also crystallize in the closed conformation (25).

It is therefore apparent that $(Ca_2)_N(Ca_2)_C$CaM has ample conformational freedom in solution, but that the extensive experimental data available do not allow us yet to make reasonable guesses on the nature and variety of the most favored conformers. Our approach is based on the exploitation of the long-range constraints that are imposed on the nuclear coordinates (pseudocontact shifts, pcs) and internuclear vector orientations (residual dipolar couplings, rdc) in one domain by the presence of paramagnetic metal ions with large and different magnetic susceptibility tensor anisotropies in the other domain. At least two metal ions are needed (26, 27) which in the present case are Tb^{3+} and Tm^{3+}. The approach capitalizes specifically on the results of recent work summarized below.

(*i*) It has been shown that lanthanide derivatives of *Drosophila melanogaster* CaM do induce appreciable pcs and rdc in the domain not bearing the lanthanide. It has been also observed that both pcs and rdc were sizably smaller than predicted by assuming that the x-ray conformation was maintained in solution, consistent with the presence of multiple conformations. The presence of a mixture of species deriving from lanthanide binding to different calcium sites apparently prevented a deeper analysis (28).

This paper was submitted directly (Track II) to the PNAS office.

Abbreviations: CaM, calmodulin; pcs, pseudocontact shifts; rdc, residual dipolar couplings; Ln, lanthanide; HSQC, heteronuclear sequential quantum correlation; NOE, nuclear Overhauser enhancement.

Data deposition: The solution structures have been deposited in the Protein Data Bank, www.pdb.org (PDB ID code 1SW8).

†To whom correspondence should be addressed at: Magnetic Resonance Center (CERM), University of Florence, Via L. Sacconi 6, 50019 Sesto Fiorentino (FI), Italy. E-mail: bertini@cerm.unifi.it.

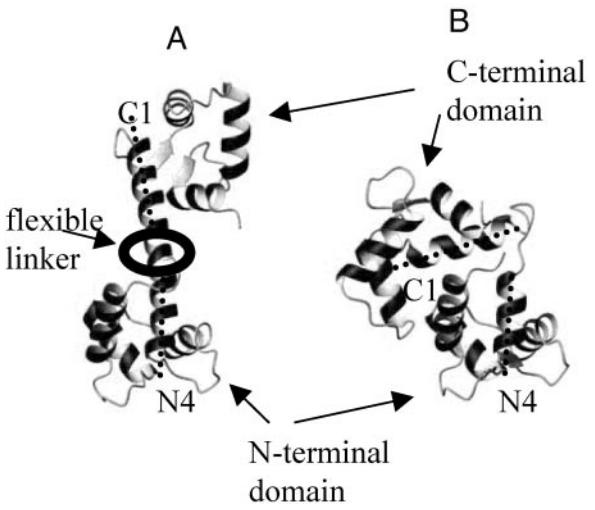

Fig. 1. Relative orientation of the N-terminal and C-terminal domains in CaM as early observed by x-ray in the absence of target peptides (*A*; extended conformation) and as observed in the presence of target peptides (*B*; closed conformation). Labels N4 and C1 indicate the fourth helix of the N-terminal domain and the first helix of the C-terminal domain, respectively.

(*ii*) An extensive series of mutants of vertebrate CaM aimed at altering the relative affinity of lanthanide (Ln) vs. calcium in the four metal binding sites was prepared and investigated by NMR. The N60D mutant was found to increase the relative affinity of calcium for the second site of the N-terminal domain to an extent that permitted the preparation of well defined $(CaLn)_N(Ca_2)_C$CaM derivatives (29).

(*iii*) The solution structure of CaM has been recently refined with an extensive use of rdc derived from an external orienting system. The structure showed significant differences in the helix orientations within the N-terminal domain with respect to the atomic resolution x-ray structure, and it provided reliable information on the orientation of internuclear vectors within both the N- and C-terminal domains (30). Therefore this structure is an essential starting point for the present study. We refer to this C-terminal domain structure as the "Bax structure." It should be noted that the information derived from the rdc obtained from an external orienting device is complicated by the fact that the orientation of each domain is the result of the contribution from the orientation of the other domain plus the direct and stronger orienting effect of the external device on the domain itself (31, 32).

Materials and Methods

Protein Expression. The plasmid pET16b-CaM was used to transform the BL21(DE3)gold *Escherichia coli* strain (Novagen) and transformants were used for the expression of unlabeled samples as previously described (29). ^{15}N-labeled N60D CaM was prepared as previously reported for unlabeled samples (29), except that immediately before induction the cells were gently pelleted and resuspended in M9 minimal medium supplemented with the appropriate isotopically labeled nitrogen (1.2 g of $^{15}NH_4Cl$ per liter) and carbon (3.5 g of [^{13}C]glucose per liter) sources. Bacterial cultures were induced with 0.5 mM isopropyl β-D-thiogalactoside, and the cells were further incubated at 37°C overnight. N60D $(Ca_2)_N(Ca_2)_C$CaM was purified as previously described (29).

Sample Preparation. After protein purification, NMR samples were prepared by buffer exchange by Centricon (Millipore) ultrafiltration with a membrane cutoff of 10,000 Da, as previously reported (29). Final conditions for NMR samples were 20 mM Mes/400 mM KCl, pH 6.5. Apo N60D CaM samples were carefully titrated up to 3 eq of Ca(II) by addition of $CaCl_2$. NMR samples (10% D_2O) were concentrated to about 1 mM protein solutions. N60D $(Ca_1)_N(Ca_2)_C$CaM samples were titrated with 50 mM solutions of analytical-grade $LnCl_3$ (Ln = Tb or Tm). The samples were kept at 4°C between measurements.

NMR Spectroscopy. NMR spectra were acquired on Bruker Avance 700 and 600 spectrometers operating at 700.13 and 600.13 MHz, respectively, equipped with triple-resonance inverse (TXI) gradient probes. Experiments were carried out at 300 K. Quadrature detection in the indirect dimensions was used and water suppression was achieved by means of WATERGATE (33). Experimental parameters are listed in Table 2, which is published as supporting information on the PNAS web site. All spectra were processed with the Bruker XWINNMR software package and analyzed by the program SPARKY (34).

pcs values of the Ln-substituted derivatives were obtained by recording ^{1}H–^{15}N heteronuclear sequential quantum correlation (HSQC) spectra (35) at 300 K and using a spectral width of 16 ppm and 32 ppm in the ^{1}H and ^{15}N dimensions, respectively. A total of 256 increments each with 1,024 complex data points and 16 transients were collected. The recycle delays were in the range between 0.7 s (paramagnetic derivative) and 1.5 s (diamagnetic derivative). pcs were calculated as the difference of the nuclear shifts between N60D $(CaLn)_N(Ca_2)_C$CaM and N60D $(Ca_1)_N(Ca_2)_C$CaM.

One-bond ^{1}H–^{15}N coupling constants were measured at 300 K and 700 MHz by fitting a series of $^1J_{NH}$-modulated HSQC spectra (36). rdc were calculated as the difference of the fitted $^1J_{NH}$ between N60D $(CaLn)_N(Ca_2)_C$CaM and N60D $(Ca_1)_N(Ca_2)_C$CaM.

Structure Calculation. Triple-resonance experiments were used to assign the backbone of N60D $(Ca_2)_N(Ca_2)_C$CaM. The backbone resonance assignment was obtained by the analysis of triple-resonance CBCANH and CBCA(CO)NH spectra (37, 38) performed at 700 MHz. Side-chain carbon and proton assignments were made by a (H)CCH-TOCSY experiment (39) at 700 MHz.

HNHA (40) and ^{1}H–^{15}N-NOESY-HSQC (41) spectra at 700 MHz allowed for torsion angle calculations. Backbone dihedral φ angles were independently derived from $^3J_{HNH\alpha}$ coupling constants through the appropriate Karplus equation. More specifically, $^3J_{HNH\alpha}$ values >7 Hz were constrained to φ angles between -155^o and -85^o and for those lower than 4.5 Hz the φ angles were constrained within -70^o and -30^o (40).

Backbone dihedral ψ angles for residue $i-1$ were also determined from the ratio of the intensities of the $d_{\alpha N}(i-1, i)$ and $d_{N\alpha}(i, i)$ nuclear Overhauser enhancements (NOEs) present on the ^{15}N(i) plane of residue i obtained from the ^{15}N-edited NOESY-HSQC. Ratio values of residue $i-1$ greater than one are indicative of β-sheets with ψ values ranging between 60^o and 180^o, whereas values smaller than one indicate a right-handed α-helix with ψ values between -60^o and -20^o (42).

NOEs were measured from 2D NOESY (43), 3D ^{1}H–^{13}C-HSQC-NOESY (41) (with a mixing time of 80 ms), and 3D ^{1}H–^{15}N-HSQC-NOESY (41) (with a mixing time of 100 ms) spectra collected at 700 MHz.

From the analysis of the 3D ^{15}N-edited and ^{13}C-edited NOESY-HSQC spectra and 2D NOESY spectrum, NOE cross-peaks were assigned and transformed into unique upper distance limits by using the program CALIBA (44). More specifically, for the N-terminal domain of N60D CaM, 2,360 NOE cross-peaks were assigned and transformed into 2,020 unique upper distance limits, of which 1,495 were found to be meaningful. For the C-terminal domain, 1,895 assigned NOEs were transformed into 1,606 unique upper distance limits and 1,225 were found to be meaningful.

The solution structure of the two domains was calculated with

Table 1. Experimental constraints collected for the N- and C-terminal domains of CaM

	No. of constraints	
	N-terminal domain	C-terminal domain
Meaningful NOEs	1,495	1,225
ϕ dihedral angles	50	43
ψ dihedral angles	50	43
pcs (Tb^{3+} and Tm^{3+})	125	165
rdc (Tb^{3+} and Tm^{3+})	—	67

the simulated annealing program DYANA (45) and PARAMAGNETIC DYANA (46).

Paramagnetism-Based Constraints. In paramagnetic metalloproteins the metal magnetic susceptibility tensor, χ^{para}, is usually anisotropic, owing to orbital contributions to the electron magnetic moment. In solution, this anisotropy produces pcs of the nuclei that are dipole–dipole coupled to the paramagnetic metal ion as well as rdc attributable to partial self-orientation (47–49). The pertinent equations are published as *Supporting Text* on the PNAS web site.

Results and Discussion

^{15}N,^{13}C-enriched vertebrate N60D $(Ca_2)_N(Ca_2)_C$CaM was subjected to the standard set of 2D and 3D experiments to assign backbone and side chains, and to obtain NOE. The relevant data are summarized in Table 1 and in Tables 3 and 4, which are published as supporting information on the PNAS web site. The structures obtained for the two domains are in good agreement with the latest solution structure refined with the help of rdc (30) resulting from orienting media (Bax structure). N60D $(CaLn)_N(Ca_2)_C$CaM derivatives with Ln = Tm or Tb were prepared, and an extensive assignment of both N-terminal and C-terminal peptide NH nuclei was performed by using a semi-automated procedure previously described (50, 51). The pcs and rdc values are summarized in Table 1 and in Tables 5 and 6, which are published as supporting information on the PNAS web site. Both pcs and rdc values of the C-terminal domain are rather small. However, they have been measured with good precision, the estimated uncertainty being ±0.05 ppm and ±0.3 Hz, respectively.

Orientations and Anisotropies of the Magnetic Susceptibility Tensors. The pcs values relative to the N-terminal domain were used together with the N-terminal atom coordinates from either the present or the Bax structure (30) to obtain the χ-tensor anisotropies and principal axes of both the Tb^{3+} and the Tm^{3+} derivatives according to a well established procedure (50, 52, 53). The best-fit values are reported in Fig. 2, where the satisfactory agreement between calculated and observed pcs is also shown (the correlation coefficient for Tb^{3+} and Tm^{3+} pcs being 0.995 and 0.987, respectively). Such good agreement can be seen as a validation of the available structures. pcs values were then provided as additional constraints to the program PARAMAGNETIC DYANA (46) together with the obtained magnetic susceptibility anisotropy values. The resulting family of solution structures of the N-terminal domain of CaM containing the N60D mutation is deposited in the Protein Data Bank (PDB ID code 1SW3).

These magnetic susceptibility anisotropy tensors determine the frame to which the positions of the C-terminal domain are referred. Such positions are referred to as *conformations* of CaM, where the N-terminal domain is fixed and the C-terminal domain is not. The very same N-terminal tensor contributes to induce a partial orientation of the N-terminal domain in a magnetic field

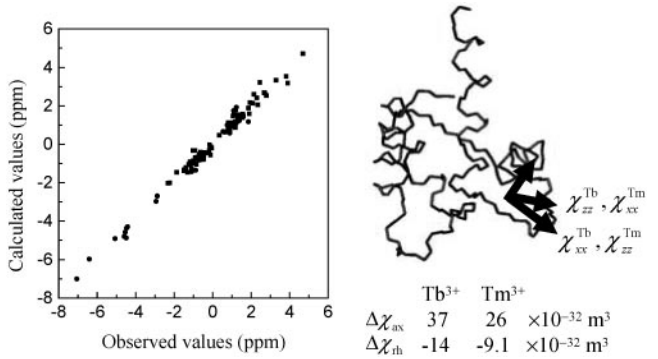

Fig. 2. Calculated vs. observed values of pcs of N-terminal nuclei for the terbium(III) (●) and thulium(III) (■) derivatives. The directions of the χ tensor axes are indicated, and the magnetic susceptibility anisotropies are reported.

and tends to induce an orientation also on the C-terminal domain. Therefore, it is possible to extract information on the relative orientation of the C-terminal and N-terminal domains.

Testing Single and Uniformly Distributed Conformations. Simple minimization programs were constructed and used to search the conformational space of CaM. One of these programs allows movements of the C-terminal domain, assumed rigid (Bax structure), relative to the N-terminal domain, also assumed rigid, through a completely flexible linker of residues 78–81 (16, 17, 23, 25). For any given conformation of the C-terminal domain, the pcs and rdc values are calculated. This program was first used to check two extreme situations: (*i*) fixed single conformations, such as those observed in the solid state, i.e., the extended and the closed forms (the latter both with and without bound target peptide or peptides); (*ii*) a uniform distribution of sterically allowed conformations.

(*i*) A large number of starting conformations was generated and used in the minimization program. In all cases, the overall agreement was poor. In particular, for the conformations observed in the solid state a poor agreement was found for both pcs and rdc, either together or separately. The pcs and particularly the rdc calculated from the x-ray conformations were much larger in absolute value than the observed ones. As expected, there is not a single CaM conformation in solution.

(*ii*) At the other extreme, a uniform distribution of all sterically allowed conformations yields average pcs values that are in reasonable agreement with the experimental ones, but average rdc values that are in disagreement with the experimental ones and show two to six times smaller spreading of values. From the latter observation we conclude that the conformational space sampled by CaM may be ample, but *the distribution must be nonuniform*. In particular, within all possible *conformations*, there must be some with less favorable *orientations* of the C-terminal domain (note that, as usual in this field, the term *orientation* is not related to the position in the reference system). The fact that not all orientations are sampled equally is an unexpected finding, whose implications will be further analyzed below.

Analysis of the C-Terminal rdc. The values and the spreading of the rdc values for the two metal derivatives may contain information on the type of rotational average experienced by the C-terminal NH vectors. Before turning to a deeper analysis of these values, we need to assess the intrinsic quality of the two sets of experimental rdc. Any set of meaningful rdc is always describable by a single orientation tensor, independently of the fact that they originate from a weighted average of a number of conformations. The latter tensor can be obtained by a simple fit of the

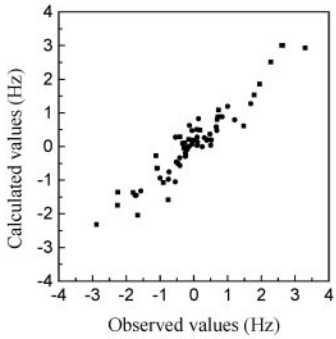

	Tb^{3+}	Tm^{3+}	
$\Delta\chi_{ax}$	−1.6	−3.3	$\times 10^{-32}$ m^3
$\Delta\chi_{rh}$	0.8	2.2	$\times 10^{-32}$ m^3

Fig. 3. Calculated vs. observed values of rdc of C-terminal HN for the terbium(III) (●) and thulium(III) (■) derivatives. Each set of data was fit separately by using FANTAORIENT.

tensor parameters to the experimental rdc and to the existing C-terminal Bax structure, using the FANTAORIENT program (48, 52). The results of the fit are shown in Fig. 3. It is apparent that a satisfactory agreement is obtained. The tensor parameter values are much smaller than those obtained from the analysis of the pcs of the N-terminal domain NH nuclei. This reduction is, of course, a consequence of extensive orientation averaging. The good agreement is a proof only of the reliability of the two rdc sets.

It is instructive to back-calculate the rdc from the full susceptibility anisotropy tensors of the two metals (case A) and from the tensors obtained above from FANTAORIENT (case B). Fig. 4*A* shows the calculated distribution of the rdc values for case A. As expected, the spreading is somewhat larger for Tb^{3+} than for Tm^{3+}, because of the larger anisotropy of the former ion. Fig. 4*B* shows the distribution of the rdc calculated for case B. For comparison purposes, Fig. 4*C* shows the calculated distribution of rdc values when averaged over all conformations except those in steric clash with the N-terminal domain. These distributions are much narrower than in case B, indicating that in the latter there must be less favorable conformations besides those prohibited by steric clashes.

It is well known that the effect of fitting to a rigid structure the rdc arising from motional averaging is that of obtaining a motionally averaged alignment tensor (54, 55). In this case, a generalized order parameter (47, 56–58) can be defined qualitatively as the ratio of the spreading between the observed rdc distribution (Fig. 4*B*) and the rdc distribution calculated in the assumption of no motion (Fig. 4*A*). Such parameter is equal to 0.05 and 0.15 for Tb and Tm rdc values, respectively. Different order parameters for the different orienting metal ions indicate that the C-terminal motion causes different motional averaging because of the different directions of the principal χ^{para} axes of the two metals (Fig. 2). This observation is further evidence that not all sterically allowed conformations are equally probable.

Search for the Least-Favored Orientations by Using C-Terminal rdc. It is known that any set of meaningful rdc values can be reproduced by a given magnetic anisotropy tensor and a weighted average of three orientations. We grid-generated all C-terminal domain orientations and, for each one, we searched for two additional orientations (described by the Euler angles) which, combined with the given one, gave the best agreement with the experimental rdc data. In some cases, the sum of the squared residuals coincided with that from the fits reported in Fig. 3, i.e., the lowest possible value; in some other cases it did not. Details of the calculation can be found in the supporting text. Such analysis indicates that, even if all orientations could be sampled by the C-terminal domain, there are regions in the orientational space

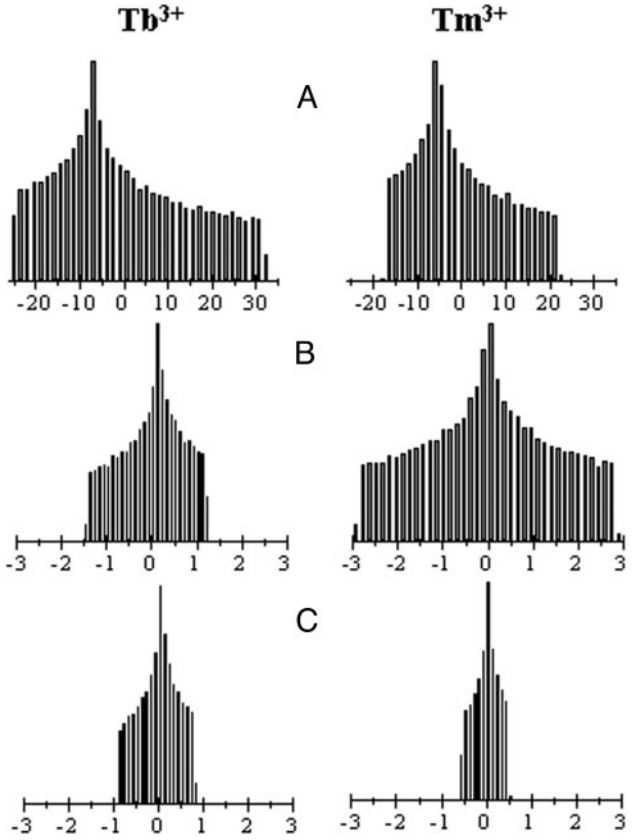

Fig. 4. Distribution of the rdc values calculated for all conformations by using the Bax structure and the magnetic susceptibility anisotropy values obtained from the experimental rdc of the N-terminal domain (*A*), from the experimental rdc of the C-terminal domain (*B*), and from the average rdc of the C-terminal domain obtained from sterically allowed uniformly sampled conformations (*C*).

less favored than others, and *these regions can be identified*. Now, we face the task of translating this information in Euler angle space into information on disfavored conformations in real Euclidean space.

Exploring the Conformational Space with C-Terminal pcs. We have mentioned that pcs calculated in either the extended or the closed conformations are not in agreement with the observed values. We then tried a six-parameter fit (three Euler angles and three translational parameters) to look for a single conformation providing a good agreement between calculated and observed values of pcs of both Tb(III) and Tm(III) simultaneously. A good fit was actually found corresponding to a conformation characterized by a tilt of the first helix of the C-terminal domain of ≈34°, with respect to the extended form, in the direction of the second metal binding site in the N-terminal domain. Such conformation has no physical meaning, as proved by the fact that the corresponding rdc are in strong disagreement with the observed values, but could be seen as a sort of "average" conformation.

If a conformation is chosen with the first helix of the C-terminal domain tilted by a large angle with respect to the extended form, as happens in the closed form where the tilt is ≈90°, a good fit is obtained for the pcs data *only* by considering other additional conformations with the interdomain helix again largely tilted, but in different directions with respect to the first one. This means that either the closed form is unfavored in

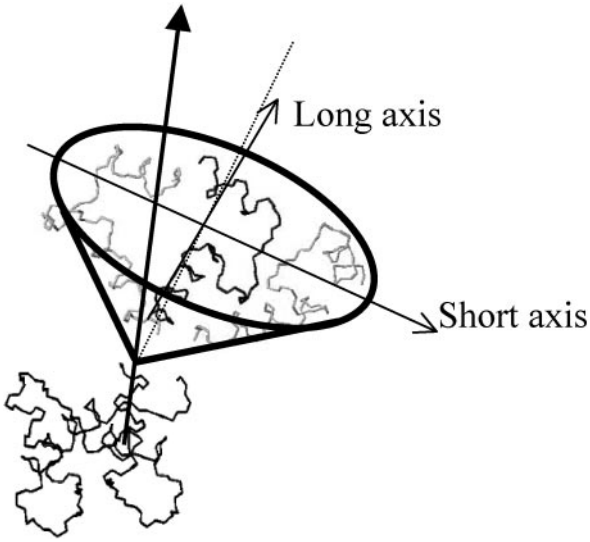

Fig. 5. Cone containing the three conformations of the C-terminal domain (only the first two helices are shown), which provide pcs and rdc with an average in good fit with the experimental data.

solution, or more than one widely different "closed" form should be present.

Minimal Sets of Conformations That Agree with Both C-Terminal rdc and pcs. pcs and rdc data were then fit simultaneously to search for the conformations providing the lowest value for the target function, keeping in mind that the lowest possible value for the target function is set by the sum of the target functions obtained from the fit performed on pcs (see *Exploring the Conformational Space with C-Terminal pcs*) and rdc (Fig. 3) (see *Analysis of the C-Terminal rdc* and *Search for the Least-Favored Orientations by Using C-Terminal rdc*) separately. The C- and N-terminal domains were held together by a completely flexible linker of residues 78–81 (16, 17, 23, 25) (such a linker was subsequently also extended to the range from residue 75 to residue 81, without significant deviations in the resulting features described below). The minimization program was then allowed to sample *triplets* of conformations with adjustable weights. The "successful" best-fit triplets provided target functions *coincident* with the lowest possible value defined above. We found a large "density" of such solutions for which the three conformations reside in an elliptical cone, whose axis is tilted by ≈30° on the direction of the second metal binding site of the N-terminal domain (Fig. 5). The major axis of the ellipsis is roughly parallel to the direction of the β-sheet located on the N-terminal domain. The fit also indicated that the C-terminal domain rotates about the axis defined by the C-terminal side of the interdomain helix. The amplitude of the semiangle of the cone ranges from 50° to 80°. Another set of calculations was performed allowing *four* conformations to be sampled. Often one of the four was with low weight, or the four were in the same region of space occupied by the conformation triplets.

To better visualize the results, we also restricted the Euler angles to assume only those values that provide orientations of the first helix of the C-terminal domain (see Fig. 1) within a fixed angle with respect to the orientation of the same helix in the extended form. This helix was thus restrained to move within a cone with fixed semiangle, and with symmetry axis along the direction of the helix in the extended form. The semiangle was set to increasing values from 10° in steps of 10°. We find that only a semiangle >40° provides a good fit. This result is due to the contribution by the rdc to the target function, as a good fit of pcs data could be obtained already for angles >10°. Another set of calculations was then performed, allowing *four* conformations to be sampled. Again, a semiangle of at least 40° was needed to provide a good fit. Such a model compares with that proposed by Baber *at al.* (17), according to which the rigid linking C-terminal helix is wobbling within a cone having a maximum semiangle of 54° with respect to the N-terminal helix.

The first helix of the C-terminal domain was then restrained to move within a cone with semiangle again variable in steps of 10°, but with the axis of the cone tilted with respect to the orientation of the same helix in the extended form. A grid search of solutions comprising three conformations was thus performed for different orientations and amplitudes of the cone. The results of the calculations show that there are indeed cones different from that depicted in Fig. 5, with semiangle larger than 40°, where it is possible to place three conformations that agree with the experimental data. In contrast, conformations inside cones with small semiangles are allowed only for the C-terminal domain bent in the same direction as that of the closed forms. We also tested the possibility that the extended form or one of the closed forms could be present among the conformations. This testing was done by searching for additional conformations that, combined with the given one, gave the best agreement with the experimental data. The result was that two additional conformations did not provide a good agreement in either case. Again, this result supports the idea that neither the extended forms nor the closed forms are particularly favored in solution. As expected, however, in both cases three additional conformations with similar weights provide a good fit.

Summary Considerations. The present research provides a further characterization of the conformational space sampled by domain reorientation of CaM by using pcs and rdc data.

The first conclusion to be drawn is that the available conformation space is quite ample and spans beyond the cone suggested by relaxation data (17). This conclusion is not in contradiction with the previous findings, as the analysis was limited to motions in the nano- to picosecond scale, whereas pcs and rdc are averaged by motions spanning a time scale that extends down to milliseconds. Apparently, slower motions than those affecting relaxation measurements may contribute to the sampling of conformational space in CaM.

The second finding is that C-terminal rdc clearly arise from averaging among very diverse orientations. Therefore, pendulum-like motions, no matter how ample, that do not imply also a rotation of the C-terminal domain about the axis of its first helix, are not sufficient in averaging the rdc down to the small values observed.

However, not all C-terminal orientations are equally probable (because the rdc would average zero), and exclusion of only those conformations in steric clash with the N-terminal domain is not enough to account for the magnitude of the observed rdc. Electrostatic repulsion between the negatively charged domains may contribute to the different probability of sterically accessible conformations.

pcs, taken alone, are seemingly less informative. It is easy to find two or more conformations, anywhere in the available conformational space, that agree with the experimental data, and even a single conformation is only in slightly worse agreement. However, there is information in this finding. The single conformation in reasonable agreement with the pcs is not far from the extended conformation (but distinct from it) and very far from the closed conformations (it is actually slightly tilted on the opposite side). As pcs depend on the reciprocal third power of the metal-nucleus distance, this finding by itself indicates that on average all nuclei of the C-terminal domain are rather far from the metal in the N-terminal domain. This in turn implies that, if a closed conformation is populated in solution, there must

be at least another similarly "closed" conformation on another side to compensate for the effect of the first.

Taken together, pcs and rdc indicate that, if motions within a cone are considered, with the exception of a few specific orientations of the axis of the cone in the direction of the closed forms, in all other orientations the cone semiangle must be at least 40° or wider. In light of the findings from relaxation data (17), we should exclude those few orientations with a too narrow cone, although they are consistent with the present data.

In conclusion, we point out that the applied procedure is of general application, as paramagnetic line broadenings decay with $1/r^6$ (r being the metal-nucleus distance), pcs decay with $1/r^3$ and rdc do not decay at all with distance. Therefore, no matter how strongly paramagnetic the metal center is, there will always be plenty of pcs and rdc to be detected outside the region of excessive broadening. For broadened lines, pcs can be measured more accurately than rdc. Therefore, if the metal sits in one domain, large and meaningful pcs can still be measured for that domain (and used to determine the tensor) while small but meaningful pcs and rdc can be measured for the other domain (and used to sample the conformational space).

Discussions with Luca Sgheri and Marco Longinetti are gratefully acknowledged. This work has been supported by the Ministero dell'Istruzione, dell'Università e della Ricerca, Italy ("Applicazioni innovative delle spettroscopie NMR ad alto campo nella ricerca industriale"), COFIN 2003 ("Il ruolo degli ioni metallici nei processi metabolici"), and by the European Commission, contract QLG2-CT-2002-00988.

1. Carafoli, E. (2002) *Proc. Natl. Acad. Sci. USA* **99,** 1115–1122.
2. Kawasaki, K. & Kretsinger, R. H. (1994) *Protein* **1,** 343–517.
3. Biekofsky, R. R., Martin, S. R., Browne, J. P., Bayley, P. M. & Feeney, J. (1998) *Biochemistry* **37,** 7617–7629.
4. Chin, D. H. & Means, A. R. (2000) *Trends Cell Biol.* **10,** 322–328.
5. Cox, J. A., Comte, M., Malnoë, A., Burger, D. & Stein, E. A. (1984) in *Metal Ions in Biological Systems: Calcium and Its Role in Biology*, ed. Sigel, H. (Dekker, NY), pp. 215–273.
6. Crivici, A. & Ikura, M. (1995) *Annu. Rev. Biophys. Biomol. Struct.* **24,** 85–116.
7. Finn, B. E., Evenäs, J., Drakenberg, T., Waltho, J., Thulin, E. & Forsén, S. (1995) *Nat. Struct. Biol.* **2,** 777–783.
8. Peersen, O. B., Madsen, T. S. & Falke, J. J. (1997) *Protein Sci.* **6,** 794–807.
9. Babu, Y. S., Bugg, C. E. & Cook, W. J. (1988) *J. Mol. Biol.* **204,** 191–204.
10. Schumacher, R. T., Rivard, A. F., Bachinger, H. P. & Adelman, J. P. (2001) *Nature* **410,** 1120–1124.
11. Ikura, M., Clore, G. M., Gronenborn, A. M., Zhu, G., Clee, C. & Bax, A. (1992) *Science* **256,** 632–638.
12. Ikura, M., Barbato, G., Klee, C. B. & Bax, A. (1992) *Cell Calcium* **13,** 391–400.
13. Meador, W. E., Means, A. R. & Quiocho, F. A. (1992) *Science* **257,** 1251–1255.
14. Osawa, M., Tokumitsu, H., Swindells, M., Kurihara, H., Orita, M., Shibanuma, T., Furuya, T. & Ikura, M. (1999) *Nat. Struct. Biol.* **6,** 819–826.
15. Elshorst, B., Hennig, M., Forsterling, H., Diener, A., Maurer, M., Schulte, P., Schwalbe, H., Griesinger, C., Krebs, J. F., Schmid, H. & Carafoli, E. (1999) *Biochemistry* **38,** 12320–12332.
16. Barbato, G., Ikura, M., Kay, L. E., Pastor, R. W. & Bax, A. (1992) *Biochemistry* **31,** 5269–5278.
17. Baber, J. L., Szabo, A. & Tjandra, N. (2001) *J. Am. Chem. Soc.* **123,** 3953–3959.
18. Seaton, B. A., Head J. F. & Richardson, F. M. (1985) *Biochemistry* **24,** 6740–6743.
19. Heidorn, D. B. & Trewhella, J. (1988) *Biochemistry* **27,** 909–915.
20. Matsushima, N., Izumi, Y., Matsuo, T., Yoshino, H., Ueki, T. & Miyake, Y. (1989) *J. Biochem. (Tokyo)* **105,** 883–887.
21. Wriggers, W., Mehler, E., Pitici, F., Weinstein, H. & Schulten, K. (1998) *Biophys. J.* **74,** 1622–1639.
22. Barton, N. P., Verma, C. S. & Caves, L. S. D. (2002) *J. Phys. Chem. B* **106,** 11036–11040.
23. Chang, S.-G., Szabo, A. & Tjandra, N. (2003) *J. Am. Chem. Soc.* **125,** 11379–11384.
24. Wilson, M. A. & Brunger, A. T. (2000) *J. Mol. Biol.* **301,** 1237–1256.
25. Fallon, J. L. & Quiocho, F. A. (2003) *Structure* **11,** 1303–1307.
26. Barbieri, R., Bertini, I., Cavallaro, G., Lee, Y.-M., Luchinat, C. & Rosato, A. (2002) *J. Am. Chem. Soc.* **124,** 5581–5587.
27. Bertini, I., Longinetti, M., Luchinat, C., Parigi, G. & Sgheri, L. (2002) *J. Biomol. NMR* **22,** 123–136.
28. Biekofsky, R. R., Muskett, F. W., Schmidt, J. M., Martin, S. R., Browne, J. P., Bayley, P. M. & Feeney, J. (1999) *FEBS Lett.* **460,** 519–526.
29. Bertini, I., Gelis, I., Katsaros, N., Luchinat, C. & Provenzani, A. (2003) *Biochemistry* **42,** 8011–8021.
30. Chou, J. J., Li, S., Klee, C. B. & Bax, A. (2001) *Nat. Struct. Biol.* **8,** 990–997.
31. Goto, N. K., Skrynnikov, N. R., Dahlquist, F. W. & Kay, L. E. (2001) *J. Mol. Biol.* **308,** 745–764.
32. Skrynnikov, N. R., Goto, N. K., Yang, D., Choy, W.-Y., Tolman, J. R., Mueller, G. A. & Kay, L. E. (2000) *J. Mol. Biol.* **295,** 1265–1273.
33. Piotto, M., Saudek, V. & Sklenar, V. (1992) *J. Biomol. NMR* **2,** 661–666.
34. Goddard, T. D. & Kneller, D. G. (2000) SPARKY 3 (Univ. of California, San Francisco).
35. Schleucher, J., Schwendinger, M., Sattler, M., Schmidt, P., Schedletzky, O., Glaser, S. J., Sorensen, O. W. & Griesinger, C. (1994) *J. Biomol. NMR* **4,** 301–306.
36. Tjandra, N., Grzesiek, S. & Bax, A. (1996) *J. Am. Chem. Soc.* **118,** 6264–6272.
37. Kay, L. E., Ikura, M., Tschudin, R. & Bax, A. (1990) *J. Magn. Reson.* **89,** 496–514.
38. Muhandiram, D. R. & Kay, L. E. (1994) *J. Magn. Reson. B* **103,** 203–216.
39. Kay, L. E., Xu, G. Y., Singer, A. U., Muhandiram, D. R. & Forman-Kay, J. D. (1993) *J. Magn. Reson. B* **101,** 333–337.
40. Vuister, G. W. & Bax, A. (1993) *J. Am. Chem. Soc.* **115,** 7772–7777.
41. Wider, G., Neri, D., Otting, G. & Wüthrich, K. (1989) *J. Magn. Reson.* **85,** 426–431.
42. Gagné, S. M., Tsuda, S., Li, M. X., Chandra, M., Smillie, L. B. & Sykes, B. D. (1994) *Protein Sci.* **3,** 1961–1974.
43. Hwang, T.-J. & Shaka, A. J. (1995) *J. Magn. Reson. A* **112,** 275–279.
44. Güntert, P., Braun, W. & Wüthrich, K. (1991) *J. Mol. Biol.* **217,** 517–530.
45. Güntert, P., Mumenthaler, C. & Wüthrich, K. (1997) *J. Mol. Biol.* **273,** 283–298.
46. Banci, L., Bertini, I., Cremonini, M. A., Gori Savellini, G., Luchinat, C., Wüthrich, K. & Güntert, P. (1998) *J. Biomol. NMR* **12,** 553–557.
47. Bertini, I., Luchinat, C. & Parigi, G. (2002) *Progr. NMR Spectrosc.* **40,** 249–273.
48. Banci, L., Bertini, I., Huber, J. G., Luchinat, C. & Rosato, A. (1998) *J. Am. Chem. Soc.* **120,** 12903–12909.
49. Bertini, I., Luchinat, C. & Parigi, G. (2001) *Solution NMR of Paramagnetic Molecules* (Elsevier, Amsterdam).
50. Allegrozzi, M., Bertini, I., Janik, M. B. L., Lee, Y.-M., Liu, G. & Luchinat, C. (2000) *J. Am. Chem. Soc.* **122,** 4154–4161.
51. Baig, I., Bertini, I., Del Bianco, C., Gupta, Y. K., Lee, Y.-M., Luchinat, C. & Quattrone, A. (2004) *Biochemistry* **43,** in press.
52. Bertini, I., Luchinat, C. & Parigi, G. (2002) *Concepts Magn. Reson.* **14,** 259–286.
53. Bertini, I., Janik, M. B. L., Lee, Y.-M., Luchinat, C. & Rosato, A. (2001) *J. Am. Chem. Soc.* **123,** 4181–4188.
54. Meiler, J., Prompers, J. J., Peti, W., Griesinger, C. & Brüschweiler, R. (2001) *J. Am. Chem. Soc.* **123,** 6098–6107.
55. Peti, W., Meiler, J., Brüschweiler, R. & Griesinger, C. (2002) *J. Am. Chem. Soc.* **124,** 5822–5833.
56. Tjandra, N. & Bax, A. (1997) *Science* **278,** 1111–1114.
57. Clore, G. M., Gronenborn, A. M. & Bax, A. (1998) *J. Magn. Reson.* **133,** 216–221.
58. Dosset, P., Hus, J. C., Marion, D. & Blackledge, M. (2001) *J. Biomol. NMR* **20,** 223–231.